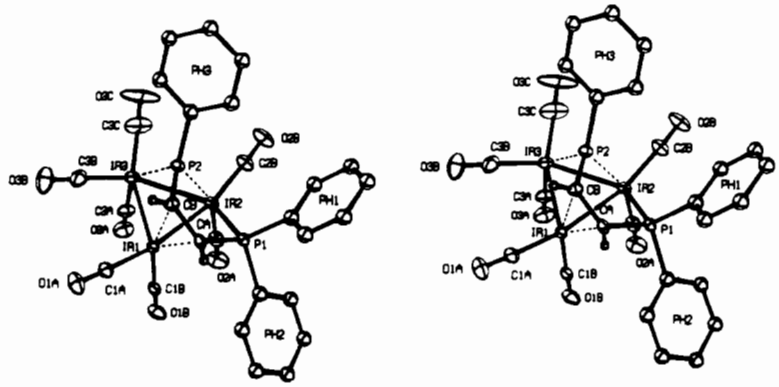

Figure 1. Stereoview of $Ir_3(CO)_7(PhPCH{=}CHPPh_2)$, illustrating the atom numbering scheme. Nonhydrogen atoms are shown as ellipsoids of 30% probability and hydrogens as spheres of radius 0.1 Å. Phenyl hydrogens are omitted for clarity.

$[H_2Ir_4(CO)_{10}]^{2-}$ (2.802 Å).[19] All of the seven carbonyls are terminal. The deviation from linearity of the Ir–C–O bonds is small, with the angles ranging from 176.1 to 179.0°.

The *cis*-$PPhCH{=}CHPPh_2$ fragment coordinates to the cluster as a tridentate ligand. P(1) coordinates to Ir(2), and P(2) bridges Ir(2) and Ir(3). The carbon–carbon double bond π bonds to Ir(1). The Ir–P bond lengths for the phosphido phosphorus, 2.289 (3) and 2.316 (3) Å, and the nonbridging phosphorus, 2.296 (3) Å, are typical of these bonding modes.[17,20] The iridium–olefinic carbon distances of 2.174 (11) and 2.183 (11) Å and the carbon–carbon distance of 1.435 (16) Å are similar to those observed for $Ir_4(CO)_5(C_8H_{12})_2(C_8H_{10})$.[21]

$Ir_3(CO)_7(\mu\text{-}(cis\text{-}PPCH{=}CHPPh_2))$ is the first known neutral triangular trinuclear iridium cluster. Although *cis*-bis(1,2-diphenylphosphino)ethane was not observed in NMR spectra of the *trans*-diphosphine starting material, the low yield of the cluster makes the source of the incorporated cis ligand uncertain—it was likely either an isomerization product of the trans ligand or formed from a minor impurity in the starting material. Synthesis of the cluster was unexpected, since the reaction of other tertiary phosphines (e.g., PPh_3, $P(p\text{-tol})_3$, and PEt_3) with $Ir(CO)_2(p\text{-toluidine})Cl$ under similar reaction conditions results in the formation of the tetranuclear clusters $Ir_4(CO)_{11}PR_3$ and $Ir_4(CO)_{10}(PR_3)_2$.

Acknowledgment. The work at Texas was supported by the Robert A. Welch Foundation (Grant No. F-233) and the National Science Foundation (Grant No. GP-37028), and the work at Delaware was supported by the donors of the Petroleum Research Fund, administered by the American Chemical Society.

Registry No. $Ir_3(CO)_7(\mu_3\text{-}(cis\text{-}PPhCH{=}CHPPh_2))$, 78149-28-7; $Ir(CO)_2(p\text{-toluidine})Cl$, 14243-22-2; *trans*-$Ph_2PCH{=}CHPPh_2$, 983-81-3.

Supplementary Material Available: A listing of observed and calculated structure factor amplitudes (27 pages). Ordering information is given on any current masthead page.

(17) D. Tranqui, A. Durif, N. Nasr Eddine, J. Lieto, J. J. Rafalko, and B. C. Gates, submitted for publication in *Inorg. Chem.*
(18) P. F. Heveldt, B. F. Johnson, J. Lewis, P. R. Raithby, and G. M. Sheldrick, *J. Chem. Soc., Chem. Commun.*, 340 (1978).
(19) G. Ciani, M. Manassero, V. G. Albano, F. Canziani, G. Giordano, S. Martinengo, and P. Chini, *J. Organomet. Chem.*, **150**, C17 (1978).
(20) (a) R. Mason, I. Sotofte, S. D. Robinson, and M. F. Uttley, *J. Organomet. Chem.*, **46**, C61 (1972); (b) P. L. Bellen, C. Benedicenti, G. Caglio, and M. Manasero, *J. Chem. Soc., Chem. Commun.*, 946 (1973).
(21) G. F. Stuntz, J. R. Shapley, and C. G. Pierpont, *Inorg. Chem.*, **17**, 2596 (1978).

Contribution from the Department of Chemistry, Cornell University, Ithaca, New York 14850

A-Frames

DAVID M. HOFFMAN and ROALD HOFFMANN*

Received November 11, 1980

The electronic structure of molecular A-frames is discussed. These are binuclear transition-metal complexes of the type $LM[\mu\text{-}E{\cdots}E]_2[\mu\text{-}X]ML$ where E···E is a bidentate ligand of the dpm or dam class and X is a bridging group such as H, Cl, S, H, CO, NO, SO_2, or acetylene. The orbitals of the invariant M_2L_6 fragment are constructed and then interacted with X. Once ambiguities in electron counting in these complexes are clarified, a consistent picture of the bonding in these molecules emerges. Among the subjects treated are metal–metal bonding in the A-frames, the possible existence of some complexes pointed to by the computed orbital patterns or isolobal analogies, and the geometrical changes at the metal centers accompanying parallel and perpendicular coordination of acetylenes.

Molecules in which two or more metal centers are held in proximity to each other, yet in which access to the metals is controlled by the ligands, offer in principle the possibility of systematic cooperative binding and activation of substrates. One such class of molecules currently under investigation comprises the so-called molecular "A-frames".[1] The A-frames are a specific set of $M_2L_6(\text{ligand})^2$ complexes with the metals held near each other by bidentate dpm or dam bridging ligands

(1) (a) Kubiak, C. P.; Eisenberg, R. *J. Am. Chem. Soc.* **1977**, *99*, 6129–6131. (b) *Inorg. Chem.* **1980**, *19*, 2726–2732.
(2) Thorn, D. L.; Hoffmann, R. *Inorg. Chem.* **1978**, *17*, 126–140.

0020-1669/81/1320-3543$01.25/0

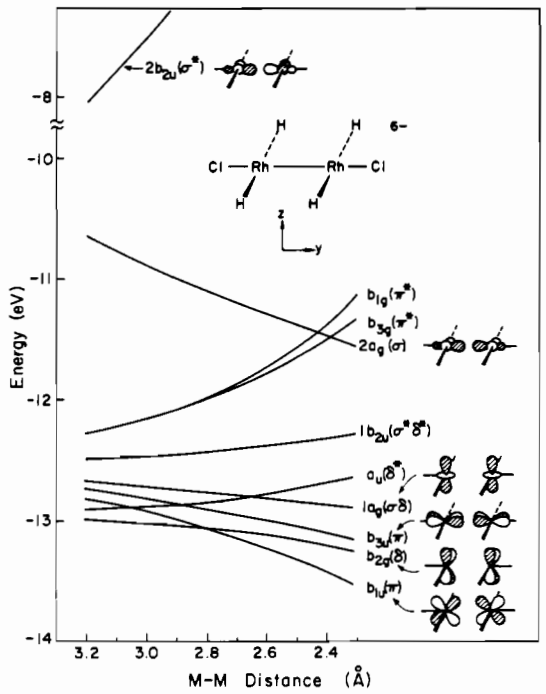

Figure 1. Frontier orbitals of planar $Rh_2Cl_2H_4^{6-}$ as the Rh–Rh distance is decreased.

(**1**) (dpm = $Ph_2PCH_2PPh_2$, dam = $Ph_2AsCH_2AsPh_2$). The idealized A-frame structure has each metal center square planar and tied together through a common ligand at the apex of the "A".

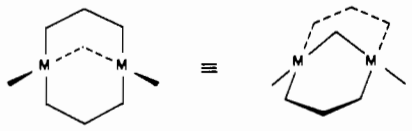

1

The structural type is quite general. The metal centers are normally Rh, Pd, or Pt. The ligands capping the "A", henceforth referred to as apex ligands, show great diversity, ranging from single-atom bridges such as S[1,3] and Cl[4] to small molecules such as CO,[5] CNR,[6] SO_2,[3,7] and C_2R_2.[8] The terminal ligands of the A-frames are typically halogens, CO, or CNR.

The electronic and geometrical structure and the reactivity of A-frames are the subjects of this paper. Our procedure will be to construct the molecular orbitals (MO's) of the appropriate M_2L_6 fragment and then interact these fragment MO's with different apex ligands. For the ligands in M_2L_6 we will use either a $H_2PCH_2PH_2$ model for dpm or a still simpler hydride ligand set. The crucial role of the bidentate ligands in conferring stability upon the actual complexes and in delimiting spatial access to the metals is clear. Nevertheless, it is our working assumption, to be tested, that the basic features of the electronic structure of the A-frames is set by the M_2L_6 coordination geometry.

All the conclusions in this contribution are based upon symmetry considerations reinforced by extended Hückel (EH) calculations, with parameters reported in the Appendix.

Orbitals of the M_2L_6 Fragment

The orbitals of the M_2L_6 fragment appropriate to the A-frames could be constructed in several ways. Perhaps the simplest procedure is to interact in a plane the orbitals of two T-shaped ML_3 fragments and then perturb the system by bending the rigid ML_3 fragments. This bending is done in such a way as to leave the M_2L_6 in the correct geometry for the A-frame complexes (i.e., such that the terminal ligand–metal–apex bridge ligand angle will be ~180°). This approach is outlined in **2**.

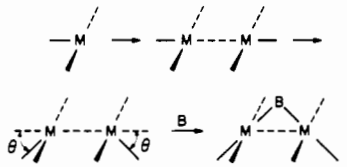

2

The basic energy ordering and orbital shape of the frontier orbitals of the T-shaped ML_3 fragment, shown in **3**, can be

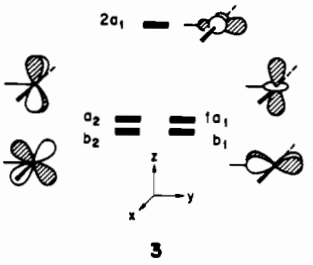

3

easily derived by using the square-planar ML_4 as a starting point.[9] Removal of a ligand L from ML_4 (along the y axis in **3**) leaves a hybrid orbital, $2a_1$, pointing toward the vacated site. In the coordinate system shown in **3**, the hybrid is composed of metal s, p, and $x^2 - y^2$. As in ML_4, below this upper orbital there are four more d-block orbitals. The relative energy ordering of these orbitals depends upon the ligands considered, but in any case they are nearly degenerate. They each reflect their ML_4 heritage and so are mainly z^2, xy, xz, and yz, respectively, in character.

To proceed toward the construction of the A-frame M_2L_6 fragment as in **2**, we show in Figure 1 the resulting 10-orbital pattern from the interaction of two MH_2Cl fragments whose M–M separation varies between 3.2 and 2.3 Å. The 10 orbitals are of course just the symmetric and antisymmetric combinations of the five orbitals given for ML_3 in **3**. The lower band of eight orbitals, $b_{1u} - b_{1g}$, is derived from the four lower orbitals of ML_3 and the two higher lying, $2a_g$ and $2b_{2u}$, from $2a_1$. We have illustrated schematically in the figure the symmetric combinations among the lower band and both $2a_g$ and $2b_{2u}$. Note also that in addition to the appropriate D_{2h} symmetry labels we have labeled the orbitals by their σ, π, or δ character.

Not unexpectedly, the orbitals symmetric with respect to reflection in the mirror plane interchanging the metals, M–M bonding, go down in energy when the M–M distance is contracted. The opposite trend is observed for the antisymmetric combinations. The most pronounced effect is on those orbitals that concentrate their orbital density between the metals, such

(3) Balch, A. L.; Benner, L. S.; Olmstead, M. M. *Inorg. Chem.* **1979**, *18*, 2996–3003.
(4) Cowie, M.; Dwight, S. K. *Inorg. Chem.* **1979**, *18*, 2700–2706.
(5) (a) Colton, R.; McCormick, M. J.; Pannan, C. D. *J. Chem. Soc., Chem. Commun.* **1977**, 823–824; *Aust. J. Chem.* **1978**, *31*, 1425–1438. (b) Brown, M. P.; Keith, A. N.; Manojlovic-Muir, Lj.; Muir, K. W.; Puddephatt, R. J.; Seddon, K. R. *Inorg. Chim. Acta* **1979**, *34*, L223–224.
(6) Olmstead, M. M.; Hope, H.; Benner, L. S.; Balch, A. L. *J. Am. Chem. Soc.* **1977**, *99*, 5502–5503.
(7) Cowie, M.; Dwight, S. K.; Sanger, A. R. *Inorg. Chim. Acta* **1978**, *31*, L407–409. Cowie, M.; Dwight, S. K. *Inorg. Chem.* **1980**, *19*, 209–216.
(8) Balch, A. L.; Lee, C. L.; Linsay, C. H.; Olmstead, M. M. *J. Organomet. Chem.* **1979**, *177*, C22–26.
(9) For other descriptions of the orbitals of this fragment see: (a) Albright, T. A.; Hoffmann, R.; Thibeault, J. C.; Thorn, D. L. *J. Am. Chem. Soc.* **1979**, *101*, 3801–3812. (b) Burdett, J. K. *Inorg. Chem.* **1975**, *14*, 375–382; *J. Chem. Soc., Faraday Trans. 2* **1974**, *70*, 1599–1613.

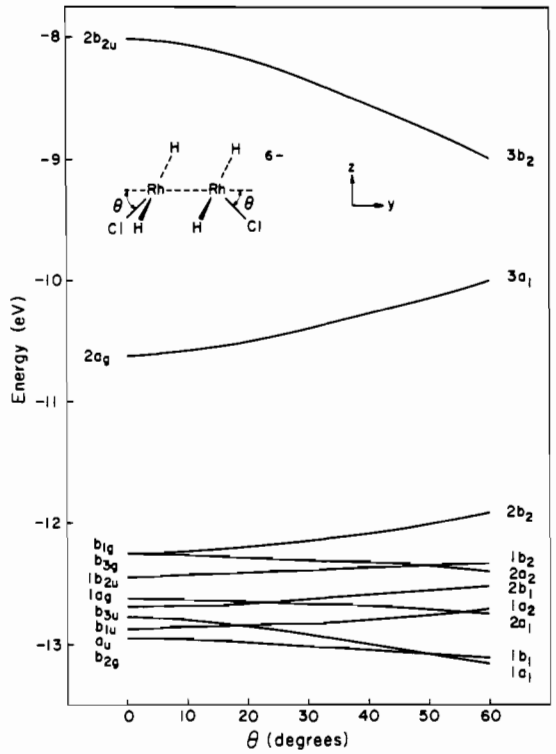

Figure 2. Evolution of the orbitals of $Rh_2Cl_2H_4^{6-}$ as θ varies. The Rh–Rh distance is 3.2 Å.

as the π,π^* and σ,σ^* orbitals. At a M–M distance typical for A-frames, about 3.2 Å, the lower eight-orbital band is tightly clustered over a 1-eV range. However, even at this relatively long M–M distance $2a_g$ and $2b_{2u}$ are split by approximately 2.6 eV. That the $2a_1$ MO's of ML_3 interact so strongly at 3.2 Å to produce this gap, while the other valence orbitals of the ML_3 fragment do not, is a reflection of the hybridization of this orbital by metal s and p mixing into $x^2 - y^2$.

While our construction of the orbitals of M_2L_6 is just a waypoint on the road to the A-frames, the level diagram of Figure 1 actually is germane to the electronic structure of a real M_2L_6 molecule, $Pt_2Cl_2(dpm)_2$ and its analogues.[10] (The M–M distance in $Pt_2Cl_2(dpm)_2$ is 2.65 Å[10a] while EH gives a minimum at 2.6 Å for the isoelectronic model $Rh_2Cl_2H_4^{6-}$.) Filling through $2a_g$ for these d^9–d^9 compounds produces a net σ-type single M–M bond.

Next we bend the L_3M–ML_3 unit. A Walsh diagram for this distortion, measured by the angle θ defined in **2**, is shown in Figure 2. This deformation, which reduces the symmetry of the M_2L_6 from D_{2h} to C_{2v}, readies the fragment for interaction with the apex ligand. The variation in θ produces only slight energy changes within the lower eight-orbital band, but the orbitals derived from $2a_g$ and $2b_{2u}$, $3a_1$ and $3b_2$, respectively, are substantially affected; $3a_1$ goes up in energy, and $3b_2$ comes down. This behavior of $3a_1$ and $3b_2$ is easily understood by examining the shape of these orbitals (Figure 1). As θ increases, overlap between the metals decreases for these orbitals, as illustrated for $3a_1$ in **4**, and this results in the M–M bonding orbital $3a_1$ being destabilized and the M–M antibonding orbital $3b_2$ being stabilized.

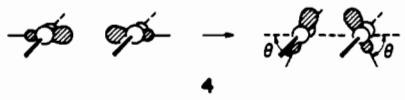

4

The shape of the 10 M_2L_6 orbitals at values of θ appropriate for the A-frames, 40–60°, is of primary interest to our analysis. The orbitals of the individual ML_3 fragments within the distorted M_2L_6 for the most part retain their shape. Thus, for instance, the deformation leaves the $3a_1$ and $3b_2$ MO's pointing toward the apex site, as illustrated for $3b_2$ in **5a**. Some of

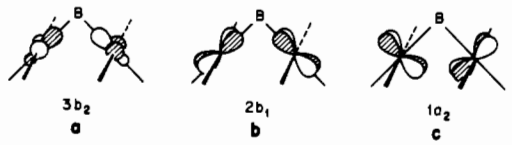

5

the orbitals of the lower band also concentrate their electron density at the apex site, e.g., $2b_1$ (**5b**), while others, like $1a_2$ (**5c**), are extended perpendicular to the ML_3 plane. These latter orbitals are better befitted to bond to ligands in the pocket of the A-frame molecule (opposite the apex bridge) or ligands binding adjacent to the apex bridge.

The considerations laid out above are in no way specific to the H_2ClRh–$RhClH_2$ model. They carry through for any M_2L_6 of the specified geometry, and in particular for Cl(dpm′)Rh–Rh(dpm′)Cl, dpm′ = $H_2PCH_2PH_2$. This is a more realistic model for an A-frame component, which we will use repeatedly in our calculations. The orbitals of such a $Rh_2Cl_2(dpm')_2$ fragment are sketched in **6**. The actual energy

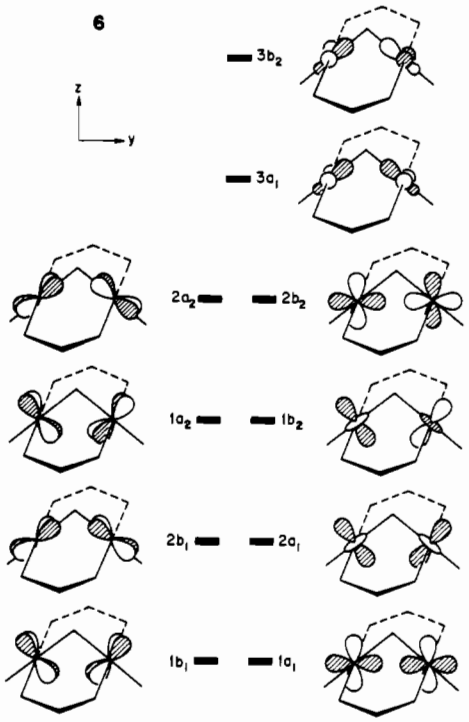

ordering of the lower eight orbitals depends upon the angle θ (see Figure 2), but the 10-orbital pattern, eight below two, is retained. Just as we described for $Rh_2Cl_2H_4^{6-}$, the two uppermost orbitals are beautifully directed in σ fashion toward the apex site. They will be most important for bonding to the ligand there. We will return to the problem of electron counting in these molecules below—for the moment it will suffice to say that for a d^8 metal, with the $Rh_2Cl_2(dpm')_2$

(10) (a) Brown, M. P.; Puddephatt, R. J.; Rashidi, M.; Manojlovic-Muir, Lj.; Muir, K. W.; Solomun, T.; Seddon, K. R. *Inorg. Chim. Acta* **1977**, *23*, L33–34. (b) Holloway, R. G.; Penfold, B. R.; Colton, R.; McCormick, M. J. *J. Chem. Soc., Chem. Commun.* **1976**, 485. (c) Manojlovic-Muir, Lj.; Muir, K. W.; Solomun, T. *J. Organomet. Chem.* **1979**, *179*, 479–491. (d) Doonan, D. J.; Balch, A. L.; Goldberg, S. Z.; Eisenberg, R.; Miller, J. S. *J. Am. Chem. Soc.* **1975**, *97*, 1961–1962. (e) Schmidbaur, H.; Mandl, J. R.; Frank, A.; Huttner, G. *Chem. Ber.* **1976**, *109*, 466–472. (f) Brown, M. P.; Fisher, J. R.; Manojlovic-Muir, Lj.; Muir, K. W.; Puddephatt, R. J.; Thomson, M. A.; Seddon, K. R. *J. Chem. Soc., Chem. Commun.* **1979**, 931–933. (g) Olmstead, M. M.; Benner, L. S.; Hope, H.; Balch, A. L. *Inorg. Chim. Acta* **1979**, *32*, 193–198.

fragment neutral, the two uppermost orbitals, $3a_1$ and $3b_2$, are free of electrons as they enter interaction with an apex fragment.

The simple picture of the M_2L_6 fragment we have presented is complicated somewhat when we consider terminal ligands other than the π donor Cl. We found that with π-acceptor terminal ligands such as CO there appear four more orbitals, a_1, a_2, b_1, and b_2, in symmetry, located in energy between $3a_1$ and $3b_2$. These are the antibonding combinations of metal d with CO π^*. Such orbitals are mainly CO π^* but in the case of the a_1 and b_2 orbitals have significant metal p and d character. The two additional a_1 and b_2 empty orbitals do serve as acceptor orbitals for the apex ligand, but, as it turns out, the bonding picture for the A-frames is not very much changed by the presence of the π acceptor (vs. π donor) as the terminal ligand. Because of this we will continue at times to refer to the M_2L_6 fragment as presenting a 10-orbital pattern of eight below two, even when CO is the terminal ligand.

We are now ready to construct the common A-frame molecules.

Single-Atom Apex Ligands

There are three single-atom-bridged A-frames for which crystal structures are available. The first reported was the sulfur-bridged $Rh_2(\mu\text{-}S)(CO)_2(dpm)_2$ (**7**).[1] Recently, crystal

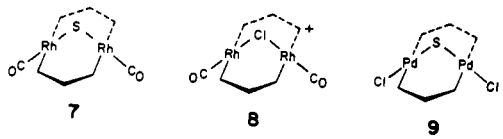

7 **8** **9**

structures of the isoelectronic compounds $Rh_2(\mu\text{-}Cl)(CO)_2(dpm)_2^+$ (**8**)[4] and $Pd_2(\mu\text{-}S)Cl_2(dpm)_2$ (**9**)[3] have been published. In each case the M–M distance is greater than 3.1 Å, and the molecular geometries are approximately that of an ideal A-frame.

Our theoretical analysis begins with $Rh_2(\mu\text{-}S)Cl_2(dpm')_2^{2-}$, isoelectronic with these molecules. In Figure 3 is shown the interaction diagram for S^{2-} with the d^8–d^8 fragment $Rh_2Cl_2(dpm')_2$. The filled p_z and p_y orbitals of the S^{2-} interact strongly with the main acceptor orbitals of the dimetal fragment, $3a_1$ and $3b_2$, respectively. In addition, the sulfur p orbitals mix with the filled a_1, b_2, and b_1 orbitals of the lower eight-orbital band. The most important of these repulsive interactions is between sulfur p_x and $2b_1$ since the antibonding combination resulting from this mixing becomes the HOMO of the A-frame molecule. The HOMO has significant sulfur p_x character (~45%).

The MO diagram of a dpm′ model for the isoelectronic compound **7**, with terminal carbonyls, is only slightly different from Figure 3. For $Rh_2(\mu\text{-}S)Cl_2(dpm')_2^{2-}$ the LUMO is mainly the antibonding combination of $3b_2$ and sulfur p_y and lies almost 5.4 eV above the HOMO. The A-frame with terminal CO ligands, however, has its LUMO ~2.9 eV above the HOMO. The reason for this difference between the two otherwise similar compounds lies in those four extra low-lying orbitals present for the M_2L_6 fragment when terminal CO's are considered. These four orbitals, as we said, are mainly CO π^* and do not interact strongly with the apex S. One of these is the LUMO of **7**.

Using Cl as an apex bridge results in a different bonding picture only in that Cl^- is a poorer donor than S^{2-}. Thus, the $2b_1$–Cl p_x repulsive interaction is not as strong as the analogous one in the μ-S case, and the A-frame b_1 MO has only ~16% Cl p_x character. The difference in the amount of apex bridge character in the higher lying filled orbitals of the μ-Cl A-frames should manifest itself in the μ-S compound showing greater nucleophilicity at sulfur. Kubiak and Eisenberg have reported that $Rh_2(\mu\text{-}S)(CO)_2(dpm)_2$ does react at the sulfur

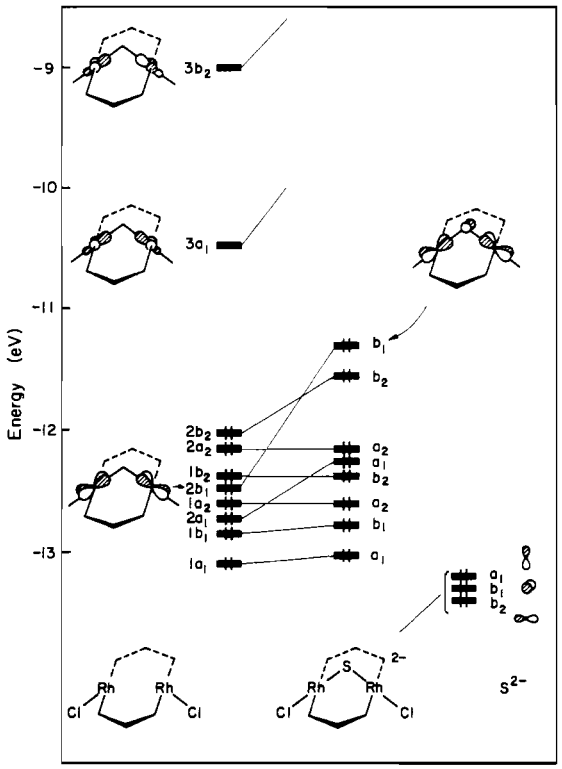

Figure 3. Orbital-interaction diagram for the model system $Rh_2(\mu\text{-}S)Cl_2(dpm')_2^{2-}$.

with electrophiles such as Et_2OR^+, R = H, Et, and that benzyl bromide effects S-alkylation.[1] The corresponding reactions for $Rh_2(\mu\text{-}Cl)(CO)_2(dpm)_2^+$ have not been reported.

We turn now to another single-atom-bridged A-frame, the μ-H complexes. Puddephatt, Seddon, and co-workers have synthesized and characterized the binuclear Pt(II) hydrides $Pt_2(\mu\text{-}H)(X)_2(dpm)_2^+$, X = Cl, CH_3, H.[11] Recently, the synthesis of the isoelectronic Rh(I) complex $Rh_2(\mu\text{-}H)(CO)_2(dpm)_2^+$ has been reported.[12]

We chose as a model μ-H A-frame $Rh_2(\mu\text{-}H)Cl_2(dpm')_2^-$ (**10**). The interaction diagram for H^- with $Rh_2Cl_2(dpm')_2$

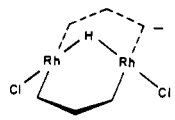

10

is shown in Figure 4. The main interaction of the hydride is with the $3a_1$ orbital of the dimetal fragment. This interaction results in substantial mixing of the $3a_1$ orbital into the filled levels of the A-frame, and as a consequence an M–M bonding interaction is precipitated. This effect will be explained in more detail and a general account given of the M–M bonding in the A-frames in the interlude that follows.

Electron Counting and Metal–Metal Bonding in A-Frames

The primary, evident geometrical feature of most A-frame complexes such as **7**–**9** is the nearly perfect square-planar coordination at the metal. One is led to think of them in terms of the square-planar, 16-electron, d^8 paradigm characteristic of complexes of the late transition metals. The electron count fits—**7** and **8** are Rh(I) dimers and **9** is a Pd(II) dimer. Given

(11) (a) Brown, M. P.; Puddephatt, R. J.; Rashidi, M.; Seddon, K. R. *Inorg. Chim. Acta* **1977**, *23*, L27–28; *J. Chem. Soc., Dalton Trans.* **1978**, 516–522. (b) Brown, M. P.; Cooper, S. J.; Frew, A. A.; Manojlovic-Muir, Lj.; Muir, K. W.; Puddephatt, R. J.; Thomson, M. A. *J. Organomet. Chem.* **1980**, *198*, C33–35.

(12) Kubiak, C. P.; Eisenberg, R. *J. Am. Chem. Soc.* **1980**, *102*, 3637–3639.

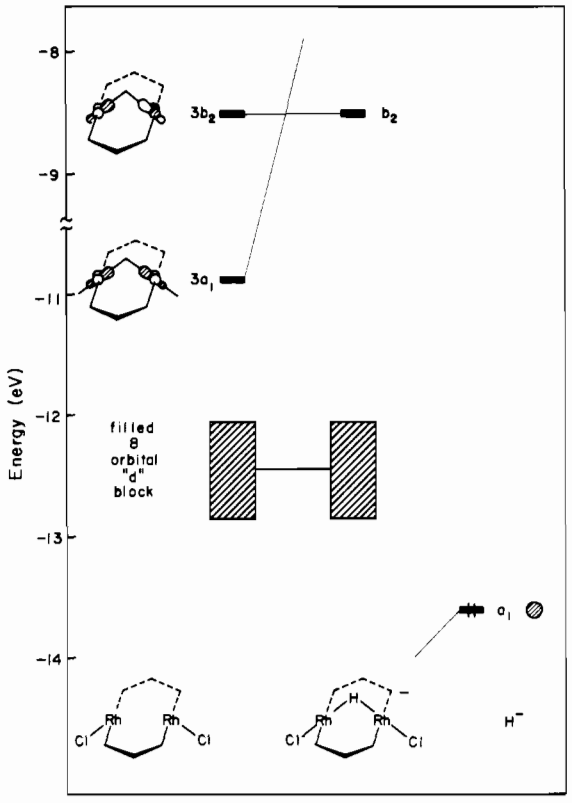

Figure 4. Orbital scheme of the model for a μ-H A-frame, $Rh_2(\mu\text{-}H)Cl_2(dpm')_2^-$.

the known propensity of such metals and oxidation states for 16-electron counts, no metal–metal interaction is imputed, and to everyone's satisfaction no evidence of such metal–metal bonding is to be found in the rather long M–M distances of 3.1–3.3 Å nor in any deformation of the local metal coordination geometry. Trouble will arise for the conventional formalism only later, when other bridging groups are considered.

Now let us see how the molecular orbital picture deals with the question of M–M bonding. In the d^8–d^8 M_2L_6 moiety the eight filled d-block orbitals contain four that are M–M bonding and four that are M–M antibonding. No formal M–M bond is expected. Yet in a calculation of Cl(dpm')Rh–Rh(dpm')Cl there is a small positive Rh–Rh overlap population of 0.064 at a Rh–Rh separation of 3.2 Å, and it rises at lower Rh–Rh distances. The origin of this small yet perhaps significant bonding is s and p mixing into the eight d-block orbitals, the same factor that is responsible for attractive interactions in some d^{10} complexes of Pt(0) or Cu(I), or for that matter for the cohesive energy of the Ni-group metals. We have analyzed this problem elsewhere.[13]

When the d^8–d^8 M_2L_6 moiety interacts with a Cl^- or S^{2-} bridge, two new bridge bonding orbitals are formed. These are shown schematically in **11**. These occupied orbitals are,

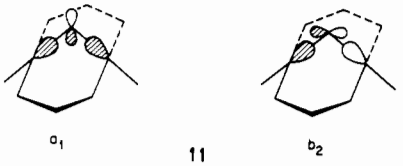

11

of course, M–X bonding. They are also perforce M–M bonding (a_1) and antibonding (b_2). The old ambiguity, traceable back all the way to diborane, arises: Are these orbitals involved in M–X bonding or in M–M bonding? The answer is "both". There is no way to shut off either type of bonding, and what happens in reality is a function of the metal, its ligands, and the bridging group.[14]

In the particular case of bridging sulfur or chloride both $3a_1$ and $3b_2$ mix with bridging-group orbitals. Both orbital types represented in **11** occur. The result might have been expected to be no change in net M–M bonding relative to the M_2L_6 fragment, since one M–M bonding orbital and one M–M antibonding orbital are occupied. In actual fact the b_2 interaction is slightly greater (to see why, one would have to analyze the relevant group overlaps[14c]) so that some net antibonding is introduced. The Rh–Rh overlap population in $Rh_2(\mu\text{-}S)Cl_2(dpm')_2^{2-}$ goes to −0.024.

We would not like to make a case for antibonding or bonding in these d^8–d^8 complexes. The net overlap population is negative but small. The M–M distances in these molecules are likely to be set by steric and packing forces rather than by electronic requirements.

The bridging hydride case is different. The complex computed is $Rh_2(\mu\text{-}H)Cl_2(dpm')_2^-$ (**10**). As Figure 4 shows, the H^- provides only a donor orbital of a_1 symmetry. The a_1 combination in **11** is occupied, not b_2. The occupied orbital is only M–M bonding, and the Rh–Rh overlap population (at the same separation that was used for Cl^- or S^{2-}) is 0.052, positive. There are thus indications of some Rh–Rh bonding. And, in fact, in a recently published structure of $Pt_2(\mu\text{-}H)(CH_3)_2(dpm)_2^+$ the metal–metal separation is shorter than in some related A-frames with nonhydride bridges.

The result of increased M–M bonding in a d^8 M_2L_6 (μ-H) A-frame would not in the least surprie a devotee of electron counting. Looking at, e.g., $Pt_2(\mu\text{-}H)Cl_2(dpm)_2^+$, he or she would count the bridging hydride as only a two-electron donor toward the two metals,[15] instead of a four-electron donor S^{2-} or Cl^-. This would lead to a d^8 Pt(II) with a 15-electron count, which in turn would call forth a metal–metal bond.

While there is no disagreement between the conclusions of the very easily applied and general electron-counting formalism and the MO approach, there might be an argument, based on simplicity, for electron counting.[16] Actually we think the molecular orbital approach is richer in its predictive detail, but to see that, we will have to develop our study further.

Small-Molecule Apex Bridges

In this section we emphasize the μ-CO and μ-SO_2 A-frames. The general bonding features revealed in these cases will also be applicable to the other A-frames with small molecules as bridges such as the N_2R,[17] CNR,[6] SR,[1,18] and PR_2[1] complexes.

The crystal structures of $Pd_2(\mu\text{-}CO)Cl_2(dam)_2$[5a] (**12**), $Pt_2(\mu\text{-}CO)Cl_2(dam)_2$[5b] (**13**), and the related $Pd_2(\mu\text{-}CNR)(CNR)_2(dpm)_2^{2+}$[6] (**14**) reveal as general structural features long M–M distances (>3.1 Å), consequently rather large M–B–M angles, and nearly square-planar metal centers. The structures do not differ in any significant way, as far as we

(13) (a) Dedieu, A.; Hoffmann, R. *J. Am. Chem. Soc.* **1978**, *100*, 2074–2079. (b) Mehrotra, P. K.; Hoffmann, R. *Inorg. Chem.* **1978**, *17*, 2187–2189.

(14) (a) Summerville, R. H.; Hoffmann, R. *J. Am. Chem. Soc.* **1976**, *98*, 7240–7254. (b) Summerville, R. H.; Hoffmann, R. *Ibid.* **1979**, *101*, 3821–3831. (c) Shaik, S.; Hoffmann, R.; Fisel, C. R.; Summerville, R. H. *Ibid.* **1980**, *102*, 4555–4572.

(15) See, however, the ideas advanced by: Berry, M.; Cooper, N. J.; Green, M. L. H.; Simpson, S. J. *J. Chem. Soc., Dalton Trans.* **1980**, 29–40.

(16) There are limitations to the electron-counting formalism. For an account of the breakdown of the correlation between bond distance and bond order deduced from the eighteen-electron rule see: Bernal, I.; Creswick, M.; Herrmann, W. A. *Z. Naturforsch. B; Anorg. Chem., Org. Chem.* **1979**, *34*, 1345–1346.

(17) Rattray, A. D.; Sutton, D. *Inorg. Chim. Acta* **1978**, *27*, L85–86.

(18) Brown, M. P.; Fisher, J. R.; Franklin, S. J.; Puddephatt, R. J.; Seddon, K. R. *J. Chem. Soc., Chem. Commun.* **1978**, 749–751. Brown, M. P.; Fisher, J. R.; Puddephatt, R. J.; Seddon, K. R. *Inorg. Chem.* **1979**, *18*, 2808–2813.

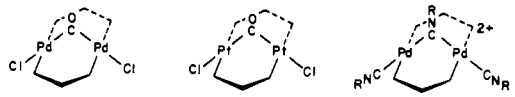

12 13 14

can perceive, from the sulfide- or chloride-bridged A-frames.

These molecules illustrate one difficulty encountered with the normal electron-counting conventions. We would all like to count a carbonyl or isocyanide as neutral, whether it is terminal, bridging, triply bridging, etc. That would lead us to the oxidation states of Pd(I) or Pt(I) in **12**–**14**. The 16-electron nature of the metal centers is retained for a neutral carbonyl bridge; **15a** is a one-electron donor to each metal.

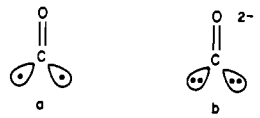

15

But we are left with the slightly uncomfortable feeling of having a d^9–d^9 dimer here, while in the Cl^-- and S^{2-}-bridged molecules we called it d^8–d^8.

All this points up the limitations of oxidation state and d-electron counting procedures, while at the same time reinforcing our feeling that there is something real or valuable about specifying the final electron count around the metal. Consistency can be restored in the present case by thinking of the bridging carbonyl as dinegative[14c] (**15b**), which makes **12**–**14** all d^8 again. More is to be learned from an orbital analysis, but for the sake of consistency we will follow this convention in the remainder of the paper.

The interaction diagram for $Rh_2(\mu\text{-}CO)Cl_2(dpm')_2^{2-}$ is displayed in Figure 5. The CO^{2-} π^* orbital of b_2 symmetry mixes strongly with the empty dimetal fragment orbital, $3b_2$, and to a lesser extent with $2b_2$. In addition, CO^{2-} π^* b_1 interacts with filled $2b_1$ and CO^{2-} a_1 with empty $3a_1$. The net result is an orbital of b_2 symmetry as the HOMO and a b_1, mainly μ-CO π^* orbital far above in energy as the LUMO.

The striking feature of the electronic structure of this molecule is a relatively high-lying HOMO of b_2 symmetry. Drawn in **16**, the HOMO resembles the $3b_2$ contribution from

16

the Rh_2 fragment, but it is directed away from the bridging ligand through mixing in $2b_2$. The $3b_2$ and $2b_2$ components make **16** net M–M antibonding—it is responsible for a −0.103 overlap population in the dimer. Since there is a relatively large gap in energy between the HOMO and the next orbital below it, it is not surprising that d^7–d^7 species, e.g., $Rh_2(\mu\text{-}CO)Br_2(dpm)_2$[19a] and the related $Rh_2(\mu\text{-}CO)Cl_2(Ph_2Ppy)_2$[19b] ($Ph_2Ppy$ = 2-(diphenylphosphino)pyridine), have been prepared. Consistent with the depopulation of the antibonding HOMO of the d^8–d^8 μ-CO A-frames (**16**), the crystal structures of these complexes reveal Rh–Rh distances of 2.76[19a] and 2.61 Å,[19b] substantially less than the Pt–Pt distance in **13** or the Pd–Pd distance in **12**. A discussion on the other structural differences between the d^8–d^8 and d^7–d^7 μ-CO A-frames is deferred until we take up the μ-SO_2 complexes.

We also looked at $Rh_2(\mu\text{-}CO)(CO)_2(dpm')_2$[12] and found the bonding features to be very similar to those shown in Figure

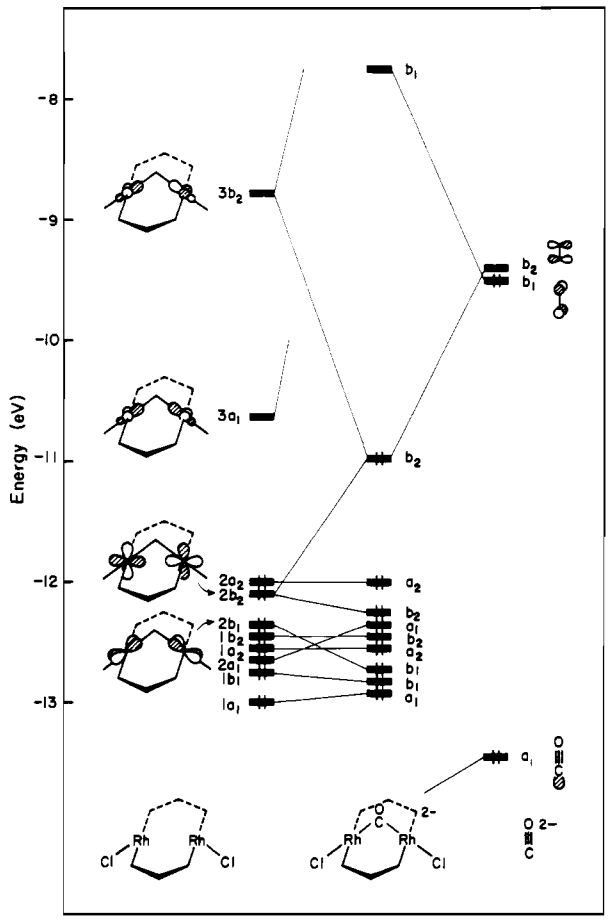

Figure 5. Interaction diagram for CO^{2-} with $Rh_2Cl_2(dpm')_2$.

5. As was the case for the μ-S compound, the terminal CO's do serve to diminish the HOMO–LUMO gap.

On the basis of our calculations of the d^8–d^8 μ-CO A-frames we would not expect a corresponding d^9–d^9 complex to be stable, at least not without a drastic change in the molecular geometry. A d^9–d^9 molecule related to the μ-CO A-frames was reported some time ago, $Ni_2(\mu\text{-}CO)(CO)_2((CF_3)_2PSP(CF_3)_2)_2$, and it has undergone a severe distortion from the A-frame-type structure (**17**).[20] The two terminal CO's of this

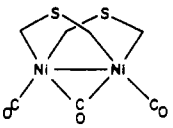

17

molecule are bent back until they are on the same side as the bridging CO. In addition the bridging diphosphine ligands are each bent away from the μ-CO. The molecule thus resembles two pseudotetrahedral Ni centers with a common ligand, the bridging CO.

Before leaving the bridging carbonyl case, we should make some remarks on the angle at the carbonyl. Bridging carbonyls of course are common in organometallic chemistry. Cotton and Hunter[21] forwarded the hypothesis that bridging carbonyls do not occur unless the bridged metal atoms are formally bonded to each other. Compound **12**, with a large MCM angle of 119°, was the first example of an exception to this generalization,[5a] and others have come to the fore since.[5b,22] It has

(19) (a) Cowie, M.; Dwight, S. K. *Inorg. Chem.* **1980**, *19*, 2508–2513. (b) Farr, J. P.; Olmstead, M. M.; Balch, A. L. *J. Am. Chem. Soc.* **1980**, *102*, 6654–6656.

(20) (a) Burg, A. B.; Sinclair, R. A. *J. Am. Chem. Soc.* **1966**, *88*, 5354–5355; *Inorg. Chem.* **1968**, *7*, 2160–2162. (b) Einspahr, H.; Donohue, J. *Ibid.* **1974**, *13*, 1839–1843.

(21) Cotton, F. A.; Hunter, D. L. *Inorg. Chem.* **1974**, *13*, 2044.

been suggested by Robinson[23] that there should be two distinct bonding modes for a bridging carbonyl. However, we feel that these are just extreme points on a continuum of M–(CO)–M interactions, which are best described in a delocalized MO picture.

A compound closely related to the μ-CO A-frame is the as yet unknown μ-NO complex. Referring back to Figure 5, the NO ligand has a lower energy π^* and so the antibonding combination between the NO $b_1\pi^*$ orbital and $2b_1$ would be expected to be lower in energy than the analogous orbital (the LUMO) of the μ-CO A-frame. In fact, a calculation on $Rh_2(\mu\text{-NO})Cl_2(dpm')_2^-$ has the b_1 MO as the LUMO but only 0.75 eV above the b_2 HOMO. Thus, a 34-electron species (b_1 filled) should be stable. On the other hand, if the 32-electron species is prepared, it may undergo some distortion to relieve this relatively small HOMO–LUMO gap. A logical motion to consider is a second-order Jahn–Teller distortion of $b_1 \times b_2 = a_2$ symmetry.[24] As shown in **18** one such motion is a

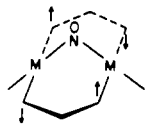

18

twist of the dpm ligands from eclipsed to staggered. Unfortunately, factors other than electronic may influence the twisting of dpm and dam ligands in the A-frames, as evidenced by the large twist seen in $Rh_2(\mu\text{-S})(CO)_2(dpm)_2$[1] but small one seen in the closely related $Rh_2(\mu\text{-Cl})(CO)_2(dpm)_2^{+}$[4] and $Pd_2(\mu\text{-S})Cl_2(dpm)_2$.[3]

We also examined two other possible distortions of the 32-electron μ-NO complex, both involving movement of the NO. One is a bend of the NO parallel to the Rh_2Cl_2 plane and the other perpendicular to it (**19a,b**). (The rest of the

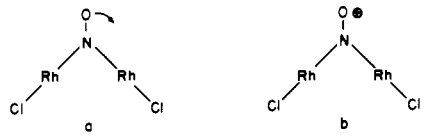

19

molecule was kept rigid for these calculations.) Both motions destabilized the complex. A deformation for which we did no calculations but that should be considered is a debridging of the NO. A complex that one might think of as an analogue of the possible end product of such a movement is $(Rh(etdp)Cl)_2$ (**20**) and similar compounds[25] (etdp = $(PhO)_2PN(Et)P(OPh)_2$).

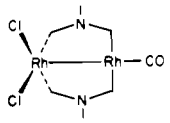

20

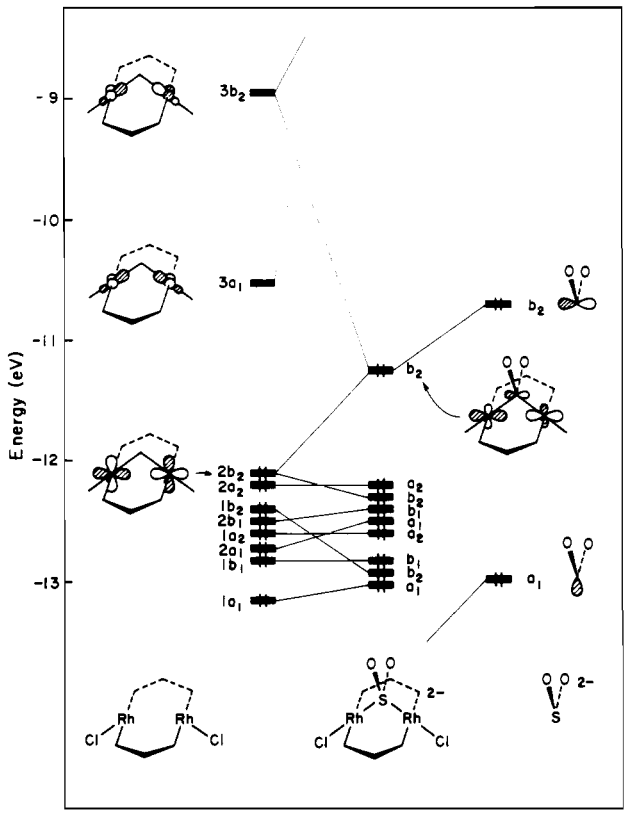

Figure 6. Orbitals of $Rh_2(\mu\text{-}SO_2)Cl_2(dpm')_2^{2-}$.

We now turn to the A-frames bridged by SO_2. Thus far, two crystal structures for μ-SO_2 A-frames have been reported, $Pd_2(\mu\text{-}SO_2)(Cl)_2(dpm)_2$[3] and $Rh_2(\mu\text{-}SO_2)(Cl)_2(dpm)_2$.[7] Balch and co-workers[3] report the Pd complex has a geometry similar to the ideal A-frame; the two independent molecules in the unit cell each have a Pd–Pd distance greater than 3.2 Å and a nearly square-planar geometry about each metal center. On the other hand, Cowie and Dwight[7] relate that the Rh complex has a deformed A-frame structure with each Rh center best described as possessing locally a highly distorted trigonal-bipyramidal structure. Most significantly the Rh–Rh distance is 2.78 Å. In **21** a geometrical comparison between the two molecules is given.

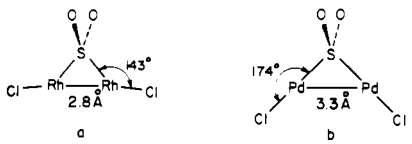

21

Figure 6 is the interaction diagram for $Rh_2(\mu\text{-}SO_2)Cl_2(dpm')_2^{2-}$, isoelectronic with **21b**. We have assumed a M–M distance of 3.2 Å and angle S–M–Cl = 180° in our calculations. We continue with the d^8–d^8 formalism and so we have SO_2^{2-} at right in the figure. In this construction, the SO_2^{2-} presents filled a_1, the lone pair, and b_2 to the $Rh_2Cl_2(dpm')_2$ fragment.[26] The lone pair of the SO_2^{2-} interacts very strongly with $3a_1$, sending the antibonding combination far up in energy. The π-donor orbital of SO_2^{2-}, mainly sulfur p_y, mixes

(22) Cowie, M.; Southern, T. G. *J. Organomet. Chem.* **1980**, *193*, C46–50.
(23) Robinson, S. D. *Inorg. Chim. Acta* **1978**, *27*, L108.
(24) (a) Den Boer, D. H. W.; Den Boer, P. D.; Longuet-Higgins, H. C. *Mol. Phys.* **1962**, *5*, 387–390. Nicholson, B. J.; Longuet-Higgins, H. C. *Ibid.* **1965**, *9*, 461–472. (b) Bader, R. F. W. *Ibid.* **1960**, *3*, 137–151; *Can. J. Chem.* **1962**, *40*, 1164–1175. (c) Bartell, L. S.; Gavin, R. M., Jr. *J. Chem. Phys.* **1968**, *48*, 2466–2483. (d) Salem, L. *Chem. Phys. Lett.* **1969**, *3*, 99–101. Salem, L.; Wright, J. S. *J. Am. Chem. Soc.* **1969**, *91*, 5947–5955. Salem, L. *Chem. Br.* **1969**, *5*, 449–458. (e) Pearson, R. G. *J. Am. Chem. Soc.* **1969**, *91*, 1252–1254, 4947–4955.
(25) (a) Haines, R. J.; Meintjies, E.; Laing, M. *Inorg. Chim. Acta* **1979**, *36*, L403–404. (b) Brown, M. P.; Cooper (neé Franklin), S. J.; Puddephatt, R. J.; Thomson, M. A.; Seddon, K. R. *J. Chem. Soc., Chem. Commun.* **1979**, 1117–1119. (c) Frew, A. A.; Manojlovic-Muir, Lj.; Muir, K. W. *Ibid.* **1980**, 624–625.
(26) (a) For some leading references on the electronic structure of SO_2 itself see: Hillier, I.; Saunders, V. R. *Chem. Phys. Lett.* **1969**, *4*, 163–164. Dacre, P. D.; Elder, M. *Theor. Chim. Acta*, **1972**, *25*, 254–258. Roos, B.; Siegbahn, P. *Ibid.* **1971**, *21*, 368–380. (b) For discussions of the electronic structure of SO_2 complexes see: Mingos, D. M. P. *Transition Met. Chem. (Weinheim, Ger.)* **1978**, *3*, 1–15. Ryan, R. R.; Eller, P. G. *Inorg. Chem.* **1976**, *15*, 494–496. Lichtenberger, D. L.; Campbell, A. C. to be submitted for publication. Ryan, R. R.; Kubas, G. J.; Moody, D. C.; Eller, P. G. to be submitted for publication.

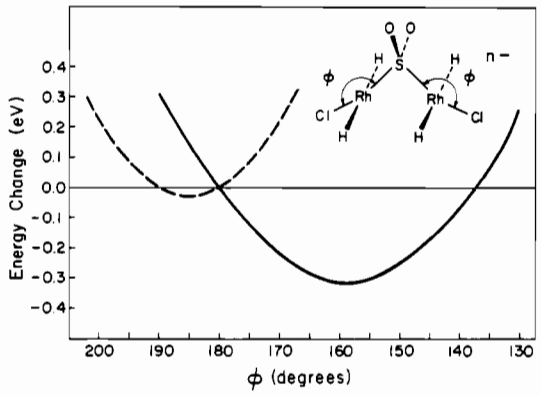

Figure 7. Change in total energy with variation of φ in $Rh_2(\mu\text{-}SO_2)Cl_2H_4^{n-}$. The dashed line is for $n = 6$ and Rh–Rh = 3.2 Å while the solid line represents $n = 4$ and Rh–Rh = 2.8 Å. $\varphi = 180°$ is taken as the arbitrary zero of energy.

strongly with both $2b_2$ and $3b_2$. The result is a three-orbital pattern of b_2 MO's in the composite molecule. In this d^8–d^8 example the second b_2 MO is filled and is the HOMO. Our calculations reveal the HOMO to be strongly M–M antibonding. This is consistent with the much contracted M–M distance found for $Rh_2(\mu\text{-}SO_2)Cl_2(dpm)_2$ (**21a**) with two electrons less.[7]

We now examine the other changes that occur in the d^8–d^8 μ-SO_2 molecule when two electrons are removed. In **21** we indicated schematically the significant differences in structure between the d^7–d^7 and d^8–d^8 molecules. The distortion of **21a** from the idealized A-frame geometry, which would have the terminal Cl ligands trans to the S, has been attributed by Cowie and Dwight[7] both to nonbonded contacts between the chloro ligands and the phenyl rings of the dpm and to the presence of the Rh–Rh bond. In order to examine the electronic contribution to the distortion more closely, we chose a simple model system, $Rh_2(\mu\text{-}SO_2)Cl_2H_4^{n-}$ (**22**) isoelectronic with $Rh_2(\mu\text{-}SO_2)Cl_2(dpm)_2$ for $n = 4$ and $Pd_2(\mu\text{-}SO_2)Cl_2(dpm)_2$ for $n = 6$.

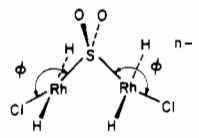

22

In Figure 7 are the total energy curves for variation of the S–Rh–Cl angle φ. For $n = 6$ and a M–M distance of 3.2 Å, EH calculations give a total energy minimum at $\varphi \simeq 187°$ while for $n = 4$ and M–M = 2.8 Å there is a minimum at $\varphi \simeq 160°$. These numbers are not in quantitative agreement with the observed structural parameters, but the trend is in the correct direction. The Walsh diagram for this deformation reveals that the highest filled b_2 orbital in Figure 6, the HOMO for $Rh_2(\mu\text{-}SO_2)Cl_2H_4^{6-}$, empty in the model with two electrons less, is responsible for the change in φ with electron count. A contour map of this orbital is given in Figure 8.

The b_2 HOMO of $Rh_2(\mu\text{-}SO_2)Cl_2H_4^{6-}$ rises sharply in energy as φ is decreased from 180°. As we mentioned earlier, this MO, the SO_2 counterpart of **16**, is M–M antibonding, M–S bonding, and M–Cl antibonding. Decrease of φ results in the M–M and M_2–SO_2 interactions being reduced while the M–Cl interaction is enhanced. The loss of M_2–SO_2 bonding and the increase in M–Cl antibonding wipe out any stabilization the orbital may have reaped from the abatement of M–M antibonding. And so the orbital is net destabilized.

The angle S–M–Cl of near 180° for the d^8–d^8 Pd complex (SO_2 counted as SO_2^{2-}!) **21b**, where the b_2 orbital is filled, is

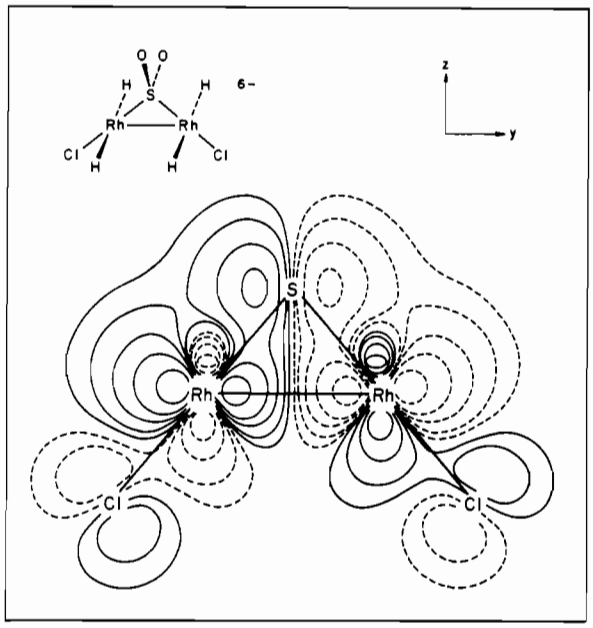

Figure 8. Contour map of the HOMO for $Rh_2(\mu\text{-}SO_2)Cl_2H_4^{6-}$ plotted in the yz plane. Rh–Rh = 2.8 Å and Cl–Rh–S = 180°. The contour levels of Ψ are ±(0.01, 0.025, 0.055, 0.10, and 0.20) in atomic units, with negative values in dashed lines and positive values as solid lines.

thus controlled by the destabilization of this orbital. When the orbital is empty, as it is for the d^7–d^7 Rh complex **21a**, the destabilization is no longer a factor. The smaller angle φ settled on in this latter case is a result of a balance between various trends in the lower filled orbitals.

The structural differences between the d^8–d^8 and d^7–d^7 μ-CO A-frames are analogous to those in the μ-SO_2 system. And, although we did not state so explicitly, the bonding picture that emerged for the μ-SO_2 complex in Figure 6 is similar to that for the μ-CO complex in Figure 5. Not surprisingly then, the electronic factors that influence the distortion of d^7–d^7 $Rh_2(\mu\text{-}CO)Br_2(dpm)_2$ from the ideal A-frame geometry[19a] are the same as those we discussed above for the μ-SO_2 compounds.

We also examined models for A-frames with apex bridging methylene, compounds synthesized and studied spectroscopically by Puddephatt and co-workers.[18] The bonding picture for the d^8–d^8 model (CH_2 counted as CH_2^{2-}!) $Rh_2(\mu\text{-}CH_2)Cl_2(dpm')_2^{2-}$ (**23**) is very similar to that for the d^8–d^8 μ-SO_2

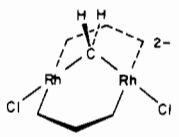

23

compound discussed above. The similarity is close enough to suggest that the d^7–d^7 species should exist, in analogy to $Rh_2(\mu\text{-}SO_2)Cl_2(dpm)_2$.

From the μ-SO_2 and μ-CH_2 A-frames one is led to examine the possibility of preparing ML_n apex bridging A-frames. It has long been recognized that d^{10} ML_2 and d^8 ML_4 both possess frontier orbitals similar to those of CH_2 in shape and energy.[27] This isolobal analogy generates, on paper, many

(27) Elian, M.; Chen, M. M. L.; Mingos, D. M. P.; Hoffmann, R. *Inorg. Chem.* **1976**, *15*, 1148–1155. Albright, T. A.; Hofmann, P.; Hoffmann, R. *J. Am. Chem. Soc.* **1977**, *99*, 7546–7557. Schilling, B. E. R.; Hoffmann, R. *Ibid.* **1979**, *101*, 3456–3466. Pinhas, A. R.; Albright, T. A.; Hofmann, P.; Hoffmann, R. *Helv. Chim. Acta* **1980**, *63*, 29–49.

interesting clusters. One example suggests that trimetal clusters such as $Pt_2(\mu\text{-}Pt(CO)_2)Cl_2(dpm)_2$ (**24**), with one long and two short M–M bonds, might be stable. We would expect that, if made, **24** and its analogues will have the $\mu\text{-}ML_2$ moiety oriented as shown.

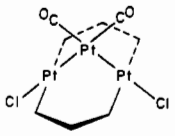

24

Apex Bridging Acetylene

Balch, Lee, Lindsay, and Olmstead have reported the synthesis and X-ray structural characterization of the acetylene A-frame $Pd_2Cl_2(dpm)_2(\mu\text{-}C_2(CF_3)_2)$[8] (**25**). The Pd complex

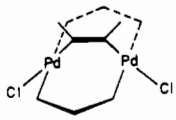

25

has a Pd–Pd distance of 3.49 Å and a nearly square-planar PdP_2ClC environment. The orientation of the acetylene in this dimetal complex, parallel to the M–M vector, is in contrast to most other dimetal acetylenes where the prevalent geometry of the acetylene is perpendicular.[28]

If we wish to pursue the square-planar, 16-electron, d^8–d^8 formalism to which the structure pushes us, we must take acetylene as a dianionic ligand $C_2H_2^{2-}$. In the sequel this will be called ac^{2-}. In preparation for the construction of an interaction diagram for acetylene bonding let us examine the orbitals of an ac^{2-}, cis bent so that the CCH angle is 124°. This bending removes the degeneracy of π and π^* and creates the four-level pattern of **26**. The first and fourth levels are unaffected by the bending; the second and third, derived from π and π^*, respectively, become hybridized. If the acetylene is taken as a dianion, three of these levels are filled, and the ac^{2-} carries a single a_2 acceptor orbital.

We will have to analyze the acetylene in two orientations, "parallel" (**27a**) and "perpendicular" (**27b**) in the sequel. It

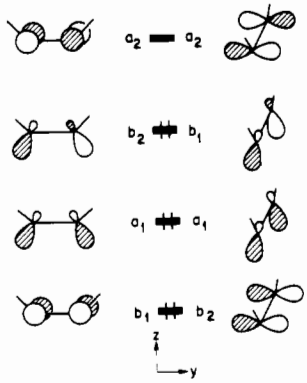

26

27

is quite arbitrary in this analysis whether one turns the acetylene or the dimetal fragment. We choose to turn the acetylene, as indicated in **26**, keeping M–M fixed. It is this (arbitrary) convention that leads to a switch in the b_1–b_2 labels of the ac^{2-} ligand levels in **26**.

Figure 9 shows an interaction diagram for ac^{2-} with $Rh_2Cl_2(dpm')_2$, in the parallel geometry that is a model for the Pd complex **25**. The filled ac^{2-} orbitals a_1 and b_2 interact most strongly with the empty dimetal fragment orbitals $3a_1$ and $3b_2$. For d^8–d^8 $M_2Cl_2(dpm')_2$ there is no low-lying acceptor orbital of b_1 symmetry and so filled acetylene b_1 mixes predominantly with the filled $2b_1$ orbital. These interactions, along with the slight mixing of acetylene a_2 with the filled $2a_2$, result in the MO picture shown in the figure.

The HOMO of the complex is the antibonding combination of acetylene b_1 and metal fragment $2b_1$. This orbital has approximately 40% acetylene character, more so than any other orbital among the eight-orbital d block. One might suspect that this orbital could be important in the hydrogenation and the cyclotrimerization of acetylene by acetylene A-frames;[8,12] this filled orbital could serve as a donor orbital for side-on attack of acetylene or H_2 (**28**).

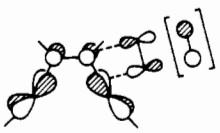

28

In Figure 10 the interaction diagram for the alternative orientation of the acetylene, perpendicular to the M–M bond, is given. To rationalize the preferred parallel configuration of the acetylene, it is easiest to focus on the interaction of the HOMO of the cis-bent acetylene dianion with the dimetal fragment. In Figure 9 the HOMO was b_2 and interacted strongly with the empty dimetal fragment $3b_2$. As we indicated in **26**, the HOMO becomes b_1 in the perpendicular configuration and so can no longer find a symmetry match among the low-lying empty dimetal fragment orbitals. It interacts intead with a filled b_1 orbital below in a four-electron repulsive interaction that sends the antibonding combination far up in energy. In addition to this repulsive interaction, the stabilization that the parallel configuration accrues from the ac^{2-} a_1–$3a_1$ mixing is partially lost in the perpendicular geometry, because the overlap is not so large between these two orbitals. These two effects result in a much higher energy for the perpendicular configuration.

(28) Some dinuclear acetylene complexes with perpendicular configurations are given in: (a) Bird, P. H.; Fraser, A. R.; Hall, D. N. *Inorg. Chem.* **1977**, *16*, 1923–1931. (b) Cotton, F. A.; Jamerson, J. D.; Stults, B. R. *J. Am. Chem. Soc.* **1976**, *98*, 1774–1779. (c) Sly, W. G. *Ibid.* **1959**, *81*, 18–20. (d) Bennett, M. A.; Johnson, R. N.; Robertson, G. B.; Turney, T. W.; Whimp, P. O. *Inorg. Chem.* **1976**, *15*, 97–107. (e) Bonnet, J.-J.; Mathieu, R. *Ibid.* **1978**, *17*, 1973–1976. (f) Wang, Y.; Coppens, P. *Ibid.* **1976**, *15*, 1122–1127. (g) Jack, T. R.; May, C. J.; Powell, J. *J. Am. Chem. Soc.* **1977**, *99*, 4707–4716. (h) Mills, O. S.; Shaw, B. W. *J. Organomet. Chem.* **1968**, *11*, 595–600. (i) Dickson, R. S.; Pain, G. N.; Mackay, M. F. *Acta Crystallogr., Sect. B* **1979**, *B35*, 2321–2325. (j) Muetterties, E. L.; Pretzer, W. R.; Thomas, M. G.; Beier, B. F.; Thorn, D. L.; Day, V. W.; Anderson, A. B. *J. Am. Chem. Soc.* **1978**, *100*, 2090–2096. (k) Green, M.; Grove, D. M.; Howard, J. A. K.; Spencer, J. L.; Stone, F. G. A. *J. Chem. Soc., Chem. Commun.* **1976**, 759–760. (l) Bailey, W. I., Jr.; Chisholm, M. H.; Cotton, F. A.; Rankel, L. A. *J. Am. Chem. Soc.* **1978**, *100*, 5764–5773. (m) Cotton, F. A.; Hall, W. T. *Inorg. Chem.* **1980**, *19*, 2354–2356. (n) Gusev, A. I.; Struchkov, Yu. T. *Zh. Strukt. Khim.* **1969**, *10*, 107–115. (o) Gusev, A. I.; Kirillova, N. I.; Struchkov, Yu. T. *Ibid.* **1970**, *11*, 62–70. (p) Fischer, E. O.; Ruhs, A.; Friedrich, P.; Huttner, G. *Angew. Chem., Int. Ed. Engl.* **1977**, *16*, 465–466. Some acetylene complexes with a parallel configuration are given in: (q) Gilmore, C. J.; Woodward, P. *J. Chem. Soc., Chem. Commun.* **1971**, 1233–1234. (r) Koie, Y.; Shinoda, S.; Saito, Y.; Fitzgerald, B. J.; Pierpont, C. G. *Inorg. Chem.* **1980**, *19*, 770–773. (s) Dickson, R. S.; Johnson, S. H.; Kirsch, H. P.; Lloyd, D. J. *Acta Crystallogr., Sect. B* **1977**, *B33*, 2057–2061. (t) Davidson, J. L.; Harrison, W.; Sharp, D. W. A.; Sim, G. A. *J. Organomet. Chem.* **1972**, *46*, C47–49.

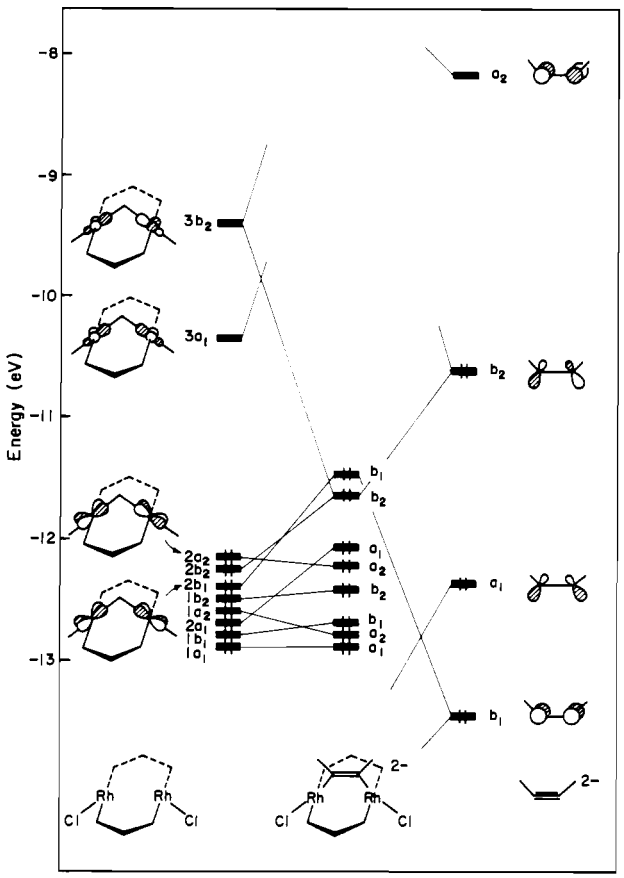

Figure 9. Interaction diagram for $Rh_2Cl_2(dpm')_2(\mu\text{-}C_2H_2)^{2-}$ in the parallel geometry. We have assumed Rh–Rh = 3.49 Å, C_{ac}–Rh–Cl = 165°, and C_{ac}–C_{ac}–H = 124°.

An M_2L_6(acetylene) complex that forms a sharp structural contrast to **25** is $Co_2(CO)_2(dam)_2(\mu\text{-}C_2Ph_2)$ (**29**).[28a] This

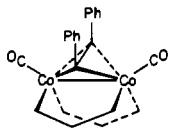

29

molecule resembles $Co_2(CO)_6(\mu\text{-}C_2\text{-}t\text{-}Bu_2)$[28b] and its analogues.[28c-h] Compound **29** has the acetylene sitting atop a "linear spine"[2] $Co_2(CO)_2(dam)_2$ fragment with the acetylene oriented perpendicular to the M–M bond.

Making a formal replacement of the d^9 (Pd–Cl) unit in **25** by a (Co–CO) unit that is also d^9 from **29** or vice versa points up the interesting structural dichotomy between **25** and **29**. In particular, the possibility of interconversion between the structural types comes to mind.

Here we examined one simple hypothetical pathway for interconverting the structural types exemplified by **25** and **29**, working with the simple model of $Co_2H_6(\mu\text{-ac})^{6-}$. The transit examined, indicated in **30**, varies many geometrical parameters

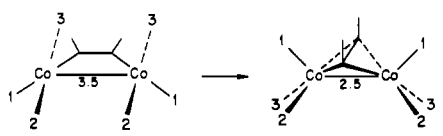

30

simultaneously. The acetylene rotates, the H_2–M–H_3 angle opens up, the Co–Co–H_1 angle changes, and the Co–Co separation decreases, all these motions coordinated so as to preserve C_2 symmetry. The correlation diagram for this motion

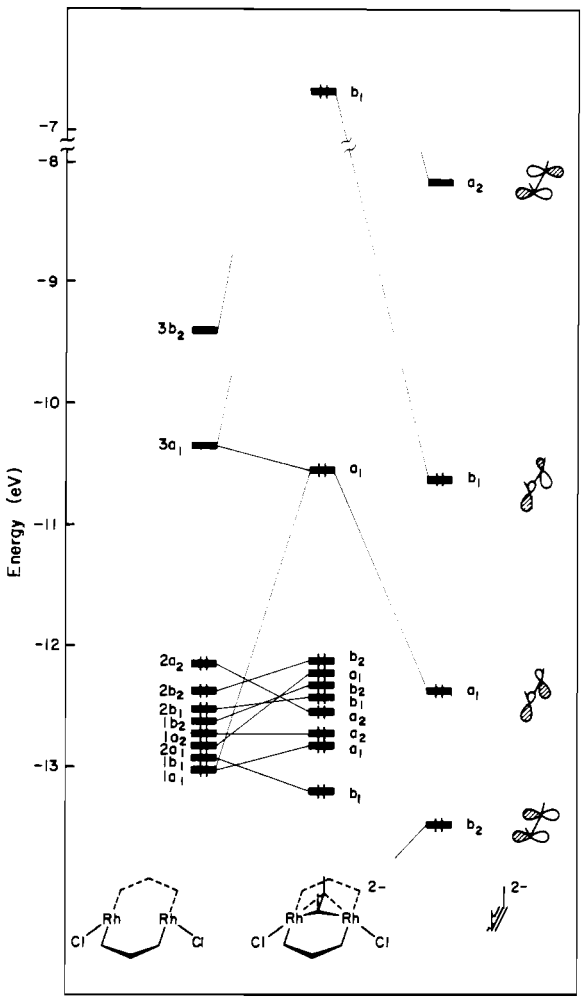

Figure 10. $Rh_2Cl_2(dpm')_2(\mu\text{-}C_2H_2)^{2-}$ in the perpendicular configuration.

shows a level crossing between the HOMO and LUMO (Figure 11). This crossing can be traced to an unfilled A-frame a_1 orbital stabilized by the loss of antibonding interaction with the hydrides and a filled b_1 destabilized by an increase in antibonding with the same ligands. This is displayed schematically in **31**.

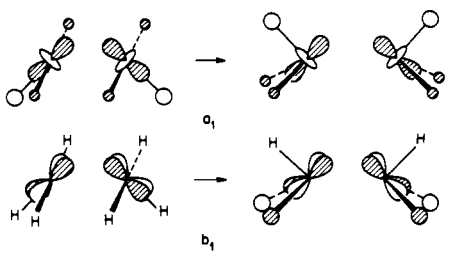

31

The structural dichotomy of **25** vs. **29** is only one of several we have noticed in the literature where the orientation of acetylene in M_2L_n(acetylene) complexes, parallel or perpendicular, is linked to large structural differences within the M_2L_n fragment. We are at present exploring the bonding in dinuclear acetylene complexes and will have more to say about the orientational preference and rotation of acetylene in these molecules in a future contribution.

From second-order Jahn–Teller reasoning and some extended Hückel calculations, we thought if two electrons were removed from the known d^8–d^8 acetylene A-frame system, **25**, it might adopt a distorted structure with the acetylene partially

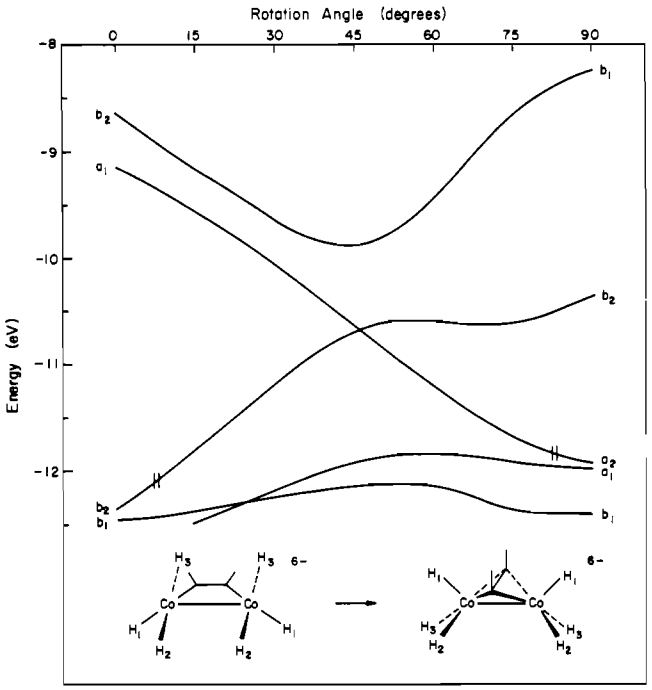

Figure 11. Correlation diagram for the interconversion of the model system $Co_2H_6(\mu\text{-}C_2H_2)^{6-}$ from the A-frame geometry to the "linear spine" geometry. The rotation angle of acetylene is indicated with 0° taken as parallel and 90° perpendicular. The Co–C_{ac} distance was kept constant at 2.0 Å for the entire motion. Perpendicular geometry includes angles Co–Co–H_1 = 152° and C–C–H = 140°.

twisted from the parallel geometry. Such is not the case. Cowie and Dickson have recently reported that the d^7–d^7 complex $Rh_2Cl_2(dpm)_2(\mu\text{-}C_2(CF_3)_2)$ (**32**) has a nearly perfect

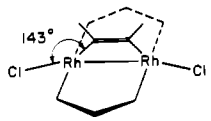

32

parallel acetylene geometry.[29,30] Complex **32** does, however, adopt a local Rh coordination geometry of distorted trigonal-bipyramidal type and forms a Rh–Rh bond.

Looking at Figure 9 for the d^8–d^8 complex, it is difficult to pick out from which orbital the electrons have come. Calculations show that it is one of the filled b_2 MO's of the composite molecule in Figure 9 that is emptied. Furthermore, we find the MO picture for our model of **32** to be similar to that shown in Figures 5 and 6 for the μ-CO and μ-SO_2 A-frames but to have two electrons less (b_2 HOMO empty). This is a reflection of the structural similarity between **32** and the d^7–d^7 μ-SO_2[7] and μ-CO[19] A-frames.[29]

Analogies to Square-Planar Complexes

Before proceeding to the doubly bridged A-frames, we wish to point out the connection between the orbitals of the square-planar ML_4 and the A-frames.[31] It is a relationship that should not be ignored since through it we can relate the A-frames to other binuclear complexes where the local metal geometry is nearly square planar such as **33**[32] and **34**.[33]

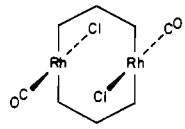

33

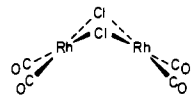

34

Each of the A-frames at which we have looked has eight filled valence orbitals, mainly metal d in character. These MO's are shown in **35**, not in any particular order of energy

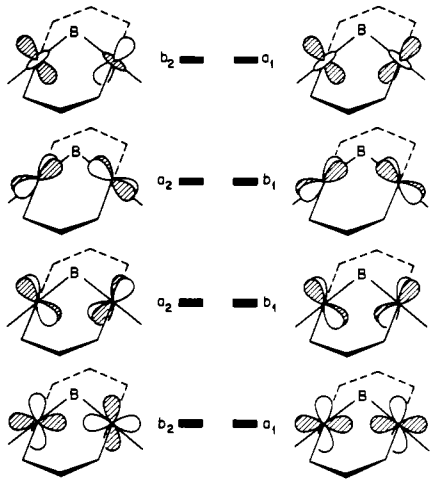

35

(for that please refer to the specific interaction diagrams) but simply as symmetric and antisymmetric combinations of metal d functions. Insofar as these are recognizable as combinations of the d orbitals of a single ML_4 d^8 complex, they will also be characteristic of the other d^8–d^8 dimers of type **33** or **34**. These orbitals, with the exception of the b_1 and a_2 orbitals pointing directly at the apex bridge, provide electron density both opposite and adjacent to the apex bridge for interaction with an electrophile.

For the single-atom-bridged A-frames these eight orbitals were the only filled MO's with significant metal d character. In the case of the μ-CO, -NO, -SO_2 and -CH_2 compounds, however, in addition to these eight orbitals the HOMO also had considerable metal d character. This orbital, shown schematically in **36**, can be related to the $x^2 - y^2$ orbital of the square-planar ML_4, but it has considerably more of its orbital density concentrated between the metal than this identification would indicate.

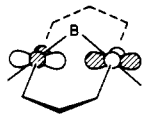

36

The ability of a d^8 ML_4 complex to pick up another base, its electrophilicity, resides in a not too high-lying orbital that

(29) Cowie, M.; Dickson, R. S., private communication.
(30) Complex **32** is an interesting structural contrast to the Cotton acetylene compound $Fe_2(CO)_6(\mu\text{-}C_2\text{-}t\text{-}Bu_2)$,[28b] where the acetylene is perpendicular and the $Fe_2(CO)_6$ resembles staggered ethane. Note again the change in metal coordination geometry that accompanies acetylene rotation.
(31) Benner, L. S.; Balch, A. L. *J. Am. Chem. Soc.* **1978**, *100*, 6099–6106.
(32) Mague, J. T. *Inorg. Chem.* **1969**, *8*, 1975–1981. Cowie, M.; Dwight, S. K. *Ibid.* **1980**, *19*, 2500–2507. For a related structure see: Mann, K. R.; Lewis, N. S.; Williams, R. M.; Gray, H. B.; Gordon, J. G., II *Ibid.* **1978**, *17*, 828–834. Balch has also done extensive studies of this type of complex: Balch, A. L. *J. Am. Chem. Soc.* **1976**, *98*, 8049–8054. Balch, A. L.; Tulyathan, B. *Inorg. Chem.* **1977**, *16*, 2840–2845. Balch, A. L.; Labadie, J. W.; Delker, G. *Ibid.* **1979**, *18*, 1224–1227.
(33) Dahl, L. F.; Martell, C.; Wampler, D. L. *J. Am. Chem. Soc.* **1961**, *83*, 1761–1762. References for other complexes of this type include: (a) Schumann, H.; Cielusek, G.; Pickardt, J. *Angew. Chem.* **1980**, *92*, 60–61. (b) Curtis, M. D.; Butler, W. M.; Greene, J. *Inorg. Chem.* **1978**, *17*, 2928–2931. (c) Bonnet, J.-J.; Kalck, P.; Poilblanc, R. *Ibid.* **1977**, *16*, 1514–1518. (d) Bonnet, J.-J.; De Montauzon, D.; Poilblanc, R.; Galy, J. *Acta Crystallogr., Sect. B* **1979**, *B35*, 832–837. Further references can be found in ref 14a.

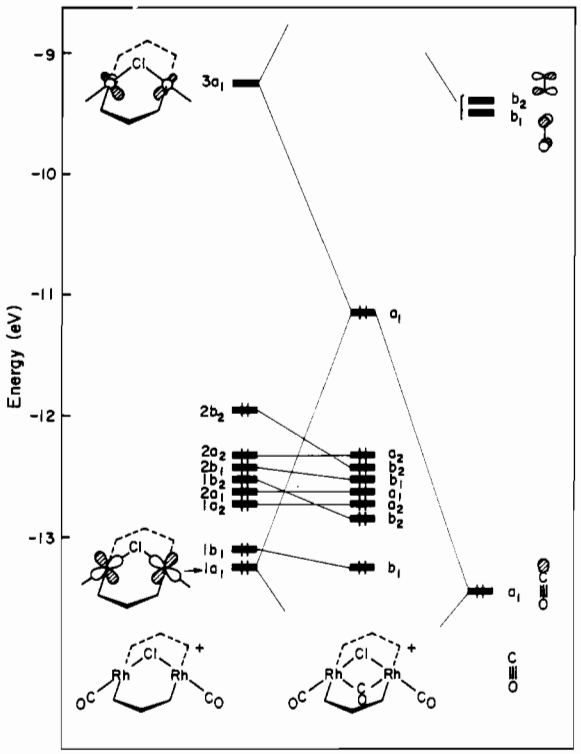

Figure 12. Interaction diagram of neutral CO with the distorted A-frame model $Rh_2(\mu\text{-Cl})(CO)_2(dpm')_2^+$.

has substantial metal p_z character, often with an admixture of acceptor π^* orbitals (**37**). The two linear combinations

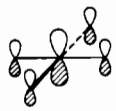

37

of such an orbital are recognizable in the A-frames but at much higher energy than the d block. We cannot say that the geometrical features of the A-frame confer any special activation on the molecule with respect to its ability to function as an electrophile. It may be that the use of good π acceptors as ligands could enhance the electrophilicity by bringing the A-frame analogues to **37** down in energy.

Doubly Bridged A-Frames

Cowie, Mague, and Sanger[34a] and, more recently, Balch and co-workers[34b] have reported the structure of $Rh_2(\mu\text{-Cl})(\mu\text{-CO})(CO)_2(dpm)_2^+$ (**38**). This compound has a Rh–Rh bond

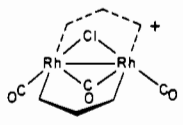

38

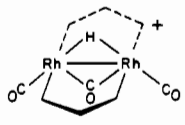

39

length of 2.84 Å and a Cl–Rh–CO (terminal) angle of 141°. Thus, the μ-Cl A-frame fragment of **38** is significantly distorted from the parent A-frame, $Rh_2(\mu\text{-Cl})(CO)_2(dpm)_2^+$, where Rh–Rh = 3.15 Å and Cl–Rh–CO = 172°.[4] The crystal structure of the isoelectronic doubly bridged A-frame $Ir_2(\mu\text{-S})(\mu\text{-CO})(CO)_2(dpm)_2$ has also been reported,[35] and its structure is similar to **38**.

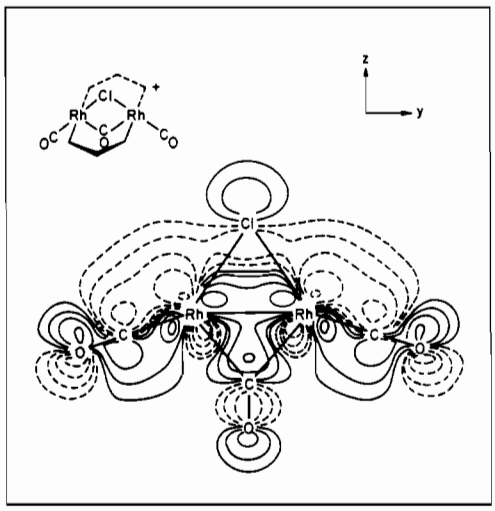

Figure 13. Contour plot of the HOMO for $Rh_2(\mu\text{-Cl})(\mu\text{-CO})(CO)_2(dpm')_2^+$ in the *yz* plane. The contour levels of Ψ are $\pm(0.01, 0.025, 0.055, 0.10,$ and $0.20)$.

Kubiak and Eisenberg have determined the molecular structure of $Rh_2(\mu\text{-H})(\mu\text{-CO})(CO)_2(dpm)_2^+$ (**39**), and it resembles **38** with Rh–Rh = 2.73 Å and H–Rh–CO = 153°.[12] The dibridged A-frames with a μ-SO_2 moiety have also been prepared.[1,7,34a,36]

Figure 12 is the interaction diagram for neutral CO[37] with the model distorted A-frame $Rh_2(\mu\text{-Cl})(CO)_2(dpm')_2^+$, where Rh–Rh = 2.78 Å and Cl–Rh–CO = 139°. The orbital pattern for the μ-Cl A-frame is somewhat different from the μ-S case at which we looked earlier (Figure 3), due primarily to the shorter M–M distance and the fact that Cl is a poorer donor than S.

The lone pair of CO interacts strongly with the filled $1a_1$ orbital of the distorted A-frame and, to a lesser degree, with empty $3a_1$. The A-frame $3a_1$ orbital is mainly terminal CO π^* but has some metal p and metal d character. The second orbital of the three-orbital pattern resulting from these interactions is the HOMO of the composite molecule. The empty CO π^* orbitals, b_1 and b_2, serve to form bonds with the appropriate filled metal orbital from the eight-orbital "d" band below ($1a_1 - 2b_2$). The orbital picture that emerges then is one in which there is a lower band of seven MO's, primarily d in character, and a somewhat removed, higher lying HOMO. The HOMO has approximately 39% d character with significant mixing of metal p (19%), terminal CO π^* (29%), and bridging CO (8%). A contour map of the HOMO is shown in Figure 13.

We also looked at the double-bridged A-frame models $Rh_2(\mu\text{-H})(\mu\text{-CO})(CO)_2(dpm')_2^+$ and $Rh_2(\mu\text{-Cl})(\mu\text{-SO}_2)(CO)_2(dpm')_2^+$ and found the bonding picture for each to be very similar to that of **38**. The isolated HOMO present in these molecules indicates that the corresponding d^7–d^7 species might be stable.

Conventional electron counting would predict a single Rh–Rh bond for **38** and no bond (perhaps a double bond) for **39**. Our calculations give an approximately equal but small bonding interaction between the metal atoms for the two complexes: the overlap populations are +0.078 for **38** and +0.057 for **39**. It is difficult to pick out any one orbital and specify that it is "the" M–M bond, but the HOMO does contribute substantially to the Rh–Rh bonding. The Rh–Rh bonds for **38** and **39** are of approximately equal length,

(34) (a) Cowie, M.; Mague, J. T.; Sanger, A. R. *J. Am. Chem. Soc.* **1978**, *100*, 3628–3629. Cowie, M. *Inorg. Chem.* **1979**, *18*, 286–292. (b) Olmstead, M. M.; Lindsay, C. H.; Benner, L. S.; Balch, A. L. *J. Organomet. Chem.* **1979**, *179*, 289–300.
(35) Kubiak, C. P.; Woodcock, C.; Eisenberg, R. *Inorg. Chem.* **1980**, *19*, 2733–2739.
(36) Mague, J. T.; Sanger, A. R. *Inorg. Chem.* **1979**, *18*, 2060–2066.
(37) We do not feel compelled in the case of the doubly bridged A-frames to count CO as the dianion as we did for the "normal" A-frames, and so we revert to the more conventional formalism.

Table I. Parameters Used in Extended Hückel Calculations

orbital	H_{ii}, eV	ζ_1	ζ_2	C_1[a]	C_2[a]
P 3s	−18.60	1.60			
3p	−14.00	1.60			
S 3s	−20.00	1.817			
3p	−13.30	1.817			
Cl 3s	−30.00	2.033			
3p	−15.00	2.033			
Rh 4d	−12.91	4.29	1.97	0.5807	0.5685
5s	−9.26	2.135			
5p	−3.88	2.10			
Co 3d	−13.18	5.55	2.10	0.5679	0.6059
4s	−9.21	2.00			
4p	−5.29	2.00			

[a] These are the coefficients in the double-ζ expansion.

whereas the simple electron-counting rules would make them of different multiplicity. The electron-counting scheme could be salvaged by treating the hydride as a pseudo-four-electron donor, as expounded by Green.[15] And the MO picture gives a still more complete description of these molecules.

The reaction chemistry of $Rh_2(\mu\text{-}Cl)(CO)_2(dpm)_2^+$ (**8**) with CO and SO_2 to form **38** and its μ-SO_2 counterpart is well studied. Cowie and co-workers[34a] report that the reaction of SO_2 occurs through attack of the ligand endo to, or directly into, the pocket of the A-frame (**40**). This is in contrast to

40

the reaction of CO, where the initial attack is exo to the pocket (**40**) and the bridging CO originates from a terminal position. While we do not have an adequate explanation for this difference in site selection between CO and SO_2, we can say that endo attack of both CO and SO_2 (coordination through S) on **8** is symmetry allowed. Furthermore, a limited surface for the approach of CO endo and exo to **8** reveals that both sites allow for substantial buildup of Rh–CO bonding.

The crystal structure of another dibridged A-frame has recently been determined, $Rh_2(\mu\text{-}C_2(CO_2Me)_2)(\mu\text{-}CO)Cl_2(dpm)_2$ (**41**).[22] This unique molecule has a long Rh–Rh

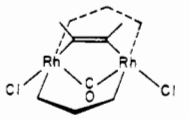

41

distance of 3.35 Å and a C_{ac}–Rh–Cl angle of 161°; the geometry of the $Rh_2Cl_2(dpm)_2(\mu$-acetylene) fragment is very similar to that for the acetylene A-frame $Pd_2Cl_2(dpm)_2(\mu\text{-}C_2(CF_3)_2)$ (**25**). A calculation on the model $Rh_2(\mu\text{-}C_2H_2)(\mu\text{-}CO)Cl_2(dpm')_2$ using the experimental geometry reveals no unusual electronic features other than a relatively low-lying isolated LUMO of a_1 symmetry (2.4 eV above the HOMO). This MO has considerable metal d and p character, with the orbital lobes protruding perpendicular to the RhP_2ClC_{ac} "plane" and away from the bridging CO. One might expect the molecule to be susceptible to nucleophilic attack at that site.

We also looked at attack of CO on $Rh_2Cl_2(dpm')_2(\mu\text{-}C_2H_2)$ (**32**) to form the dibridged species. A correlation diagram for the endo attack of CO (**40**) assuming C_{2v} symmetry (least motion) indicates this pathway to be symmetry forbidden. A non-least-motion endo attack is likely.

Acknowledgment. The impetus for this work came from several discussions with R. Eisenberg. We are grateful to J. Jorgensen for the drawings and E. Stolz for the typing. The National Science Foundation generously supported this work through Research Grants CHE 7828048 and DMR-7681083 to the Materials Science Center at Cornell University.

Appendix

All calculations were performed by using the extended Hückel method,[38] with weighted H_{ij}'s.[39] Unless otherwise mentioned, in our calculations of the A-frames we assumed a terminal ligand–metal–apex ligand angle of 180° and a Rh–Rh distance of 3.2 Å. Other bond distances used throughout were as follows: C–H, 1.09 Å; P–H, 1.44 Å; C–O, 1.16 Å; M–H, 1.7 Å; Rh–P, 2.3 Å; Rh–terminal CO, 1.81 Å; Rh–terminal Cl, 2.34 Å. The Rh–apex ligand distances were taken from the actual crystal structures when available.

The parameters used in our calculations are listed in Table I. The parameters for C, N, O, and H are the standard ones.[38] Rh exponents and all Co parameters have been used previously.[14b] H_{ii}'s for Rh were obtained from a charge iteration on $Rh_2(\mu\text{-}Cl)(\mu\text{-}CO)Cl_2(dpm')_2^+$ assuming a quadratic charge dependence for the Rh H_{ii}'s.[40] The charge iteration parameters are from Baranovskii and Nikol'skii.[41]

(38) Hoffmann, R. *J. Chem. Phys.* **1963**, *39*, 1397–1412. Hoffmann, R.; Lipscomb, W. N. *Ibid.* **1962**, *36*, 2179–2195, 2872–2883.
(39) Ammeter, J. H.; Bürgi, H. B.; Thibeault, J. C.; Hoffmann, R. *J. Am. Chem. Soc.* **1978**, *100*, 3686–3692.
(40) Basch, H.; Viste, A.; Gray, H. B. *Theor. Chim. Acta* **1965**, *3*, 458–464.
(41) Baranovskii, V. I.; Nikol'skii, A. B. *Teor. Eksp. Khim.* **1967**, *3*, 527–533.